Manufacturable Conducting Rubber Ambers and Stretchable Conductors from Copper Nanowire Aerogel Monoliths

Yue Tang,[†,‡] Shu Gong,[†,‡] Yi Chen,[†] Lim Wei Yap,[†] and Wenlong Cheng[†,‡,*]

[†]Department of Chemical Engineering, Monash University, Clayton, Victoria 3800, Australia, and [‡]The Melbourne Centre for Nanofabrication, 151 Wellington Road, Clayton, Victoria 3168, Australia

ABSTRACT We report on a low-cost, simple yet efficient strategy to fabricate ultralightweight aerogel monoliths and conducting rubber ambers from copper nanowires (CuNWs). A trace amount of poly(vinyl alcohol) (PVA) substantially improved the mechanical robustness and elasticity of the CuNW aerogel while maintaining a high electrical conductivity. The resistivity was highly responsive to strains manifesting two distinct domains, and both followed a power law function consistent with pressure-controlled percolation theory. However, the values of the exponents were much less than the predicted value for 3D systems, which may be due to highly porous structures. Remarkably, the CuNW-PVA aerogels could be further embedded into PDMS resin, forming conducting rubber ambers. The ambers could be further manufactured simply by cutting into any arbitrary 1D, 2D, and 3D shapes, which were all intrinsically conductive without the need of external prewiring, a condition required in the previous aerogel-based conductors. The outstanding electrical conductivity in conjunction with high mechanical compliance enabled prototypes of the elastic piezoresistivity switches and stretchable conductors.

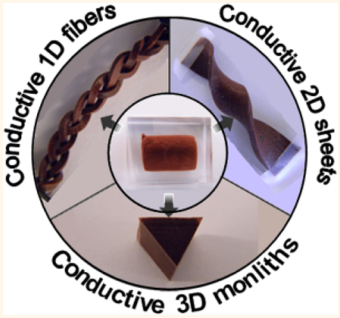

KEYWORDS: copper nanowires · aerogel · conducting rubber ambers · stretchable conductors · piezoresistivity

Foldable and stretchable conductors are a new class of advanced materials that can maintain high conductivity under various deformations, including bending,[1] stretching,[2] compressing,[3] and twisting.[4] This type of conductor has implications in a wide spectrum of technological fields,[5] including electronic paper,[6] flexible displays,[7] touch screens,[8] artificial skins,[9−11] and implantable medical devices.[12] Over the past several years, substantial progress has been made in designing flexible conductors with diverse materials, such as carbon nanotubes,[13] graphene,[14] conductive polymers,[15] semiconducting nanostructures,[16,17] metal oxides,[18] metallic nanoparticles,[19−21] and metal nanowires.[1,22,23]

Despite the exciting progress, some of the aforementioned materials will unavoidably face cost or low-abundance issues in terms of downstream practical real-world applications. For example, the success in metal nanomaterials-based flexible conductors was predominantly limited to precious gold or silver nanowires.[1,19,20] Despite their outstanding performances, copper nanowires (CuNWs) may offer cost benefits for commercial applications of flexible conductors because of the high copper abundance on earth.[24] Compared to cheaper commercial conducting fillers such as carbon particles, CuNWs may lead to better conductivity due to the high intrinsic bulk conductivity of copper. However, copper nanomaterials are largely under-explored in fabrication of flexible conductors due to their high tendency for oxidation and low solvent dispersion.[25]

In a previous work, we have successfully fabricated ultralightweight aerogel monoliths from CuNWs, which could exhibit high conductivities even when their densities were about 1/1000 of bulk copper.[26] However, the poor mechanical stability prevented CuNWs aerogel monoliths from being used as foldable and stretchable conductors. Herein, we show a trace amount of additive—poly(vinyl alcohol) (PVA)—could substantially improve the mechanical strength of CuNW aerogels while maintaining high conductivity (~0.83 $S \cdot cm^{-1}$) and ultralow density (~10 $mg \cdot cm^{-3}$). The CuNW−PVA composite aerogels exhibited high durability at cyclic loads, enabling their applications as an elastic piezoresistivity

* Address correspondence to wenlong.cheng@monash.edu.

Received for review January 16, 2014 and accepted May 26, 2014.

Published online May 29, 2014
10.1021/nn502702a

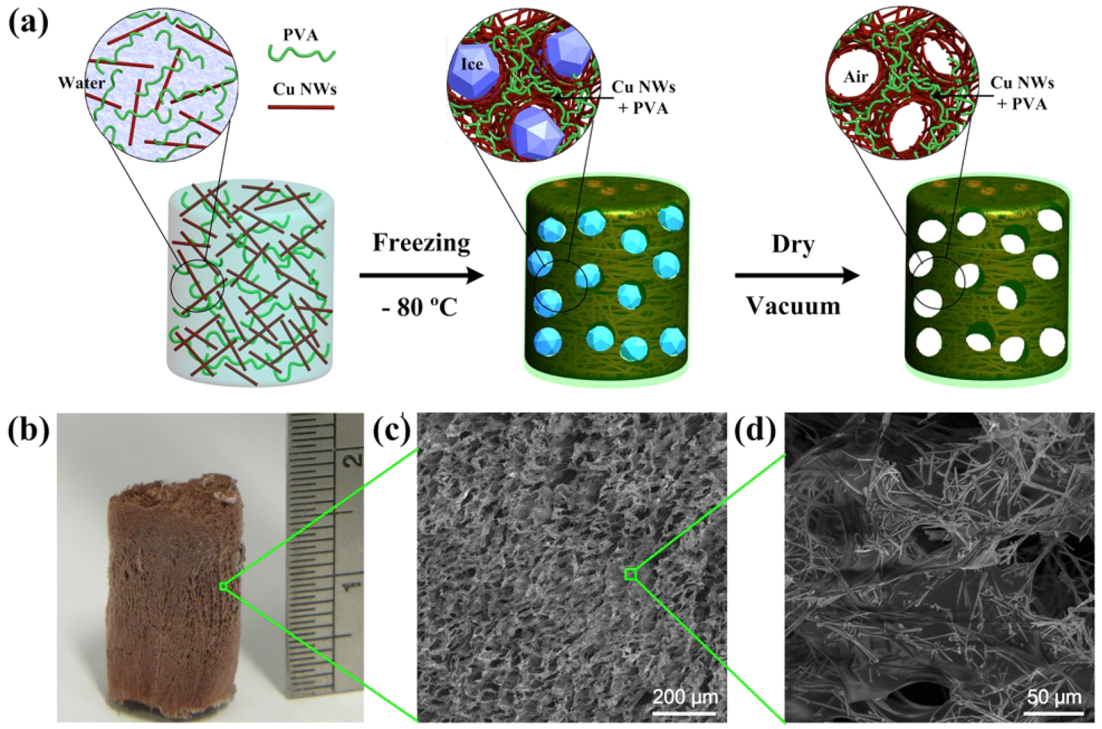

Figure 1. Large-scale fabrication of CuNW–PVA composite aerogel monoliths: (a) schematic illustration of the synthesis process; (b) photographic image; (c and d) SEM images at different magnifications.

switch. More importantly, the CuNW–PVA aerogels could be embedded into a polydimethylsiloxane (PDMS) matrix, leading to electrically conductive rubber ambers without the need of prewiring, which was required in the previous aerogel-based conductors.[1,13,27] PVA played a critical nanogluing role, preventing CuNW conducting networks from collapsing during PDMS embedding, therefore maintaining high conductivity. Notably, the rubber ambers could be further manufactured into various one-dimensional (1D), 2D, and 3D objects that were all conductive after cutting. We believe that our fabrication strategy represents a new low-cost route to manufacture under mild conditions flexible conductors with versatile shapes for versatile applications in flexible electronics.

RESULTS AND DISCUSSION

To fabricate CuNW–PVA aerogel monoliths and conducing rubber ambers, we began with synthesis of CuNWs following the published protocols.[25,26] Briefly, $Cu(NO_3)_2$ was mixed with hydrazine and ethylenediamine under strong basic conditions. Then CuNWs were grown in an ice bath in the presence of polyvinylpyrrolidone (PVP), which prevented the CuNWs from aggregating. The as-produced nanowires have typical dimensions of 60 nm × 20 μm. Next, the CuNWs were purified by repeated centrifugation and redispersion in PVA aqueous solutions, which were followed by a freeze-drying process as illustrated in Figure 1a. This led to the formation of highly porous CuNW–PVA composite aerogel monoliths labeled as CuNW–PVA (*x*), where *x* stands for the concentration of PVA in units of $mg \cdot L^{-1}$.

Figure 1b shows the photographic image of a typical cylindrical CuNW–PVA (10) composite aerogel monolith that has a density of only 9.6 $mg \cdot cm^{-3}$. Further characterizations by scanning electron microscopy demonstrated highly porous, interconnected tubular structures (Figure 1c and d). In contrast, broken tube-like structures were observed in the CuNW aerogel monoliths (Figure S1b). Unlike previously reported polymer–silver composite aerogels where individual metallic nanowires are wrapped by polymers,[28] it appears that the PVA polymers existed throughout the entire 3D scaffolds of CuNWs (Figure 1d). Despite this, the entire aerogel remained highly conductive with a conductivity of 0.83 $S \cdot cm^{-1}$, only about 26% lower than the conductivity for the corresponding CuNW aerogel monoliths without PVA. Furthermore, we found that the electrical conductivity of the CuNW–PVA composite aerogels could be enhanced to 8.1 $S \cdot cm^{-1}$ by mild annealing at 80 °C, which is comparable to conductive aerogels composed of metallic nanostructures or carbon materials.[14,29]

PVA substantially improved the mechanical robustness and flexibility of CuNW aerogels, allowing for large deformations without fracturing. In one demonstration, a CuNW–PVA (10) composite aerogel could almost return to its original height (Figure 2a) after a compressive strain up to 60%; in contrast, the corresponding CuNW aerogel without PVA demonstrated little height recovery (<5%). Figure 2b shows the

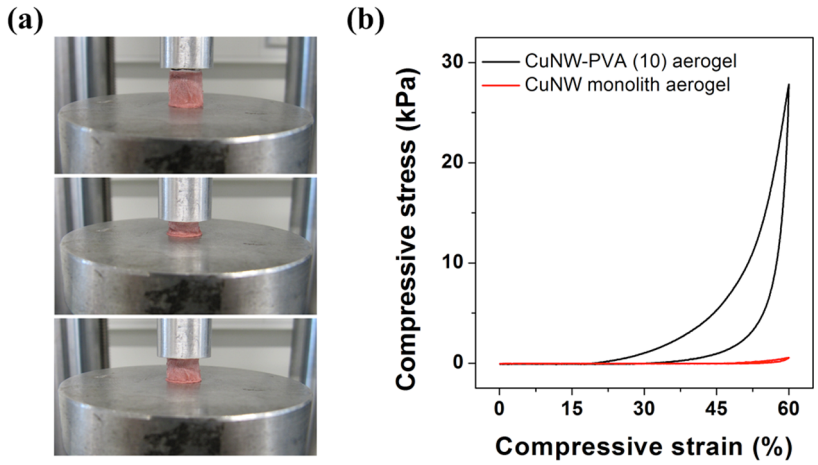

Figure 2. Mechanical properties of CuNW–PVA composite aerogel monoliths. (a) Snapshot photographic images of CuNW–PVA (10) composite aerogels under compressing and shape recovery. (b) Compressive stress–strain curves of CuNW–PVA (10) composite aerogels (black line) and CuNW monolith aerogels (red line) at the compressive strain of 60%.

TABLE 1. Effect of PVA on Density, Electrical Conductivity, Young's Modulus, and Elasticity of CuNW Aerogel Monoliths

	CuNW aerogel monoliths	CuNW–PVA (10) composite aerogels	CuNW–PVA (15) composite aerogels	CuNW–PVA (20) composite aerogels
density ($mg \cdot cm^{-3}$)	9.4 ± 0.9	9.6 ± 0.2	9.9 ± 0.3	10.1 ± 0.6
Young's modulus (Pa)	5.88	159.87	286.90	545.69
electrical conductivity ($S \cdot cm^{-1}$)	1.13	0.83	0.39	0.29
elasticity	×	√	√	√

comparison of stress–strain curves for CuNW and CuNW–PVA (10) for the second compression cycle. Note that the stress–strain curve for CuNW–PVA (10) featured a plateau region followed by a steep region. In the plateau region, compressive stress gradually increased with the strain, indicating elastic deformation; in the steep regions, the stress increased rapidly with the strain owing to the densification of porous structures.[3] The Young's moduli of CuNW aerogel monoliths increased with the increasing amount of PVA added (Figure S2). Nevertheless, the increase of PVA addition did not result in much decrease in conductivity (Figure S3).

We systematically investigated the effect of PVA concentration, *x*, on density, Young's modulus,and electrical conductivity of CuNW–PVA composite aerogels as summarized in Table 1. By varying concentration, *x*, from 0 to 20 $mg \cdot L^{-1}$, the density of the aerogel increased only slightly up to a maximum of ~7% from ~9.4 $mg \cdot cm^{-3}$ to ~10.1 $mg \cdot cm^{-3}$; the electrical conductivity decreased by about 4 times from ~1.13 $S \cdot cm^{-1}$ to 0.29 $S \cdot cm^{-1}$; however, the Young's modulus of the composite aerogel increased up to 93 times from 5.88 Pa to 545.69 Pa.

The outstanding mechanical and electrical properties of the CuNW–PVA aerogel monoliths originate from their unique internal structures. Loosely bound CuNWs could not sufficiently maintain the porous frameworks during the freeze-drying process, especially in the case of aerogels from low concentrations of CuNWs, leading to the observation of broken tubular structures (Figure S1b). This led to low elasticity due to the low efficiency in load transfer among broken tubular structures. In contrast, in the presence of PVA, highly porous CuNWs frameworks were largely maintained (Figure 1c and d). PVA served as "nanoglue", effectively fixing the CuNW junction structures in place and promoting the load transfer throughout the networks. This explains the dramatic enhancement in mechanical properties observed in this work (Table 1). Interestingly, it appears that PVA did not break the ohmic contacts between CuNWs but wrapped their junction points. Therefore, the conductivity of the aerogel did not decrease much after introducing PVA (Table 1). Note that the role of PVA (*i.e.*, nanogluing effects) in our aerogel was fundamentally different from that in the previous composite aerogels,[28,30] in which PVA conformably coated individual nanowires to exhibit nanocabling effects in their electrical properties.

The excellent conductivity in conjunction with high mechanical compliance exhibited by our CuNW–PVA composite aerogels indicated their potential applications in flexible electronics. Figure 3a shows the changes of electrical resistance under compressive stress for CuNW–PVA (20). Note that the electrical resistance decreased rapidly in the initial stage of compression and then reached a plateau after a strain

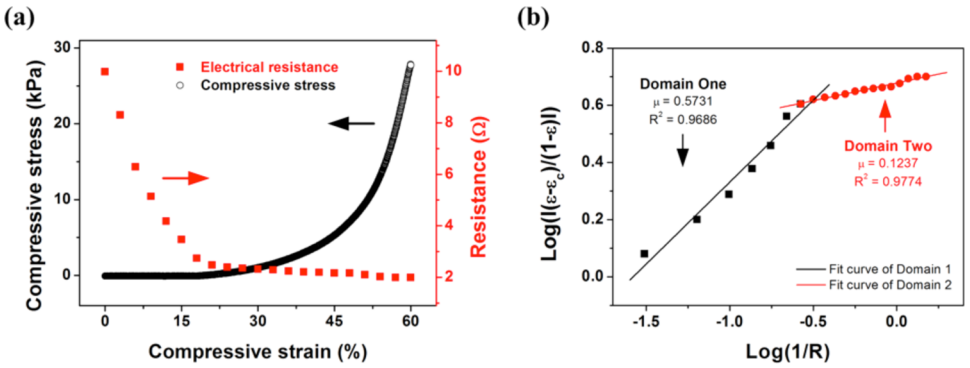

Figure 3. Electrical properties of CuNW−PVA composite aerogels under compressive strains. (a) Plots of electrical resistance and compressive stress as a function of compressive strains for the CuNW−PVA (20) composite aerogel monolith. (b) Plots of $|(\varepsilon - \varepsilon_c)/(1 - \varepsilon)|$ *versus* $1/R$ in logarithmic scale. The black curve represents the linear fitting of data points (black) in domain 1, and the red curve is the fitting of the data points (red) in domain 2. Note that $1/R$ is proportional to σ and $1/R_c$ is proportional to σ_c.

of about 30%. This may originate from pressure-driven percolation conductivity.[31] The overall conductivity of the composite aerogel, σ, depends on the effective volume fraction of CuNWs (the ratio of total volume of CuNWs to the total volume of the deformed aerogel). We consider an initially nonconductive homogeneous insulator matrix uniformly doped with conductive materials.

The pressure-controlled percolation conductivity in terms of strain can be written as a power law function:[31]

$$\sigma(\varepsilon)_{\varepsilon>\varepsilon_c} \propto \sigma_c \left| \frac{\varepsilon - \varepsilon_c}{1 - \varepsilon} \right|^{\mu}$$

where $\sigma(\varepsilon)$ is the conductivity at the stress ε, σ_c is the conductivity percolation threshold at the stress ε_c, and μ is the conductivity exponent. Now we assume our CuNW−PVA aerogel monolith obeys this theory and that $\varepsilon_c = 0$ since all our CuNW−PVA aerogels were conductive without any compressive stress. The results presented in Figure 3b manifest two evident domains with different exponents of the power law, −0.57 and 0.12. The excellent linear relationships validate the percolation theory. However, the values of the exponents are much less than the predicted $\mu = 2.0$ for 3D systems. The apparent discrepancy in conductivity exponents could be understood since our systems were far beyond the conductivity percolation threshold. Interestingly, clear sharp transitions in Figure 3a and b demonstrated the presence of another "conductivity threshold". This may be attributed to the percolation of porous structures under compressive stress: the conductivity in domain 1 may be due to the deformation of pores accompanying squeezing air out the matrix; the conductivity in domain 2 may be due to the densification of CuNWs like the normal homogeneous insulator matrix far beyond the conductivity percolation threshold.

For the more conductive CuNW aerogels, the resistance change became less sensitive to strain (Figure S4). In particular, the resistance of CuNW−PVA composite aerogels with an electrical conductivity of 0.29 $\Omega \cdot cm^{-1}$ decreased by 400% at the compressive strain of 60%; in contrast, electrical resistance of composite aerogels with an electrical conductivity of 1.8 $\Omega \cdot cm^{-1}$ decreased by only around 10% of the original value. It is expected that more stress-resistant conductivity could be achieved with more conductive aerogels.

The stress-induced resistance changes were consistent in loading−unloading cycles except for the first loading−unloading cycle (Figure S5). The partial breaking of the conductive percolation network in the first loading step may cause different resistance changes in the first loading−unloading cycle. For the following loading−unloading cycles, the resistance changes became consistent.

The unique piezoresistivity properties enabled our CuNW−PVA composite aerogels to directly serve as elastomeric resistor switches. To illustrate the capability, a CuNW−PVA (20) composite aerogel was sandwiched between two conducting silver paste-coated glass slides to form a resistor. The resistor was then connected to light-emitting diodes (LEDs) and batteries in series. As shown in Figure S6 inset and supplementary video 1, upon pressing, the aerogel LED lamps became brighter and upon release the lamps returned to dim. This is due to the piezoresistive effects described above. Under compressive stress, the resistance of the aerogel decreases, leaving more partial voltage to the LED lamps to make them brighter; upon releasing, the elastic aerogel returned to the original shape and recovered its large resistance, leaving less partial voltage to the LED lamps to make them dim again.

Quantitative pressure-induced resistance changes are shown in Figure 4a. The sensitivity of our aerogel sensor can be defined as $S = \delta(\Delta R/R_{off})/\delta P$, where ΔR is the relative change in resistance, R_{off} is resistance of the sensor under no load, and δP is the change in applied pressure. Thus, the slopes in the low- and

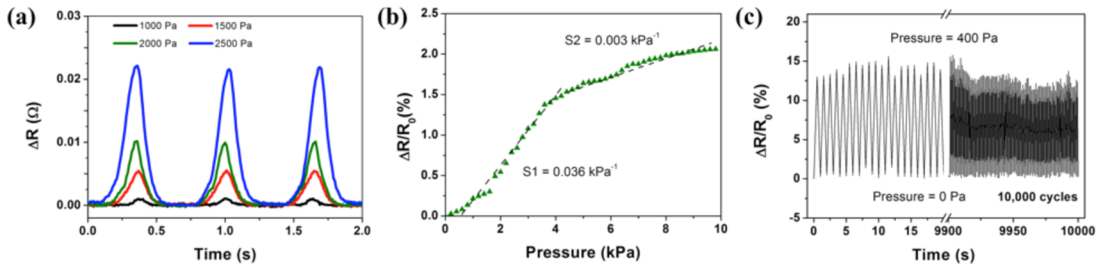

Figure 4. Resistive pressure response of CuNW–PVA composite aerogels. (a) Multiple-cycle tests of repeated loading and unloading pressure ranging from 1 to 2.5 kPa. (b) Resistance change as a function of applied pressure. (c) Durability test of CuNW–PVA (10) composite aerogels under repeated loading and unloading pressures of 400 Pa. Note that the variation of the electrical resistance was still stable after 10 000 loading–unloading cycles. The frequency was 1.0 Hz.

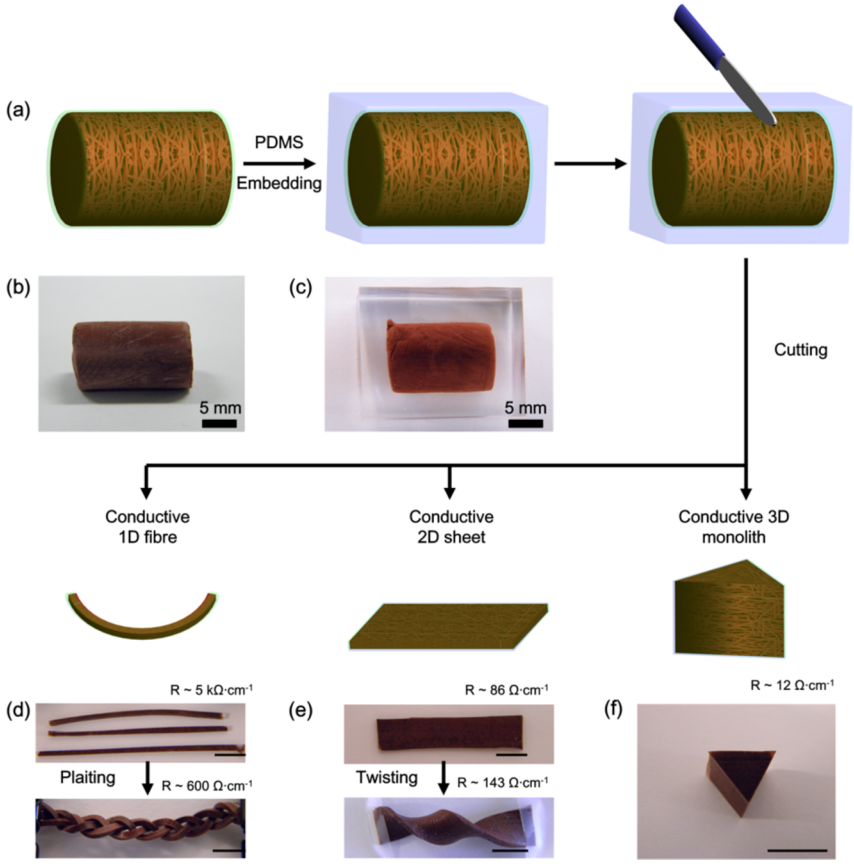

Figure 5. Manufacturability of the conducting rubber ambers by simple knife cutting. (a) Schematic of the amber-fabrication process and the follow-up cut-shaping process. (b and c) Photographic images of CuNW–PVA aerogel monoliths before (b) and after (c) PDMS embedding. (d–f) Cut-shaped 1D, 2D, and 3D structures. All the cut-shaped rubbers were conductive. The scale bar was 1 cm.

high-pressure regions in Figure 4b gave a sensitivity of 0.036 and 0.003 kPa^{-1}. The devices are not as sensitive as our previous gold nanowire-based wearable sensors,[23] but they do not require expensive materials or expensive microfabrication tools for interdigitated electrode arrays. Our devices were also less sensitive than graphene-based pressure sensors,[32] but they offer advantages such as low-cost materials, mild materials processing, fewer processing steps, and no need for additional supporting matrix. In addition, we also tested device durability. As shown in Figure 4c, pressure-induced changes in resistance are repeatable for >10 000 loading–unloading cycles, comparable to the previously reported pressure sensors.[32]

Another unique attribute is that our CuNW–PVA aerogels could be embedded into a PDMS matrix to form conducting rubber ambers without the need of prewiring (Figure 5a). PVA played a critical nanogluing role in preventing CuNW scaffolds from collapsing during embedding, therefore enabling maintaining the high conductivity. In a control experiment, directly embedding a CuNW aerogel into PDMS led to an insulated rubber amber. The aerogels were mechanically robust, and no deformation was observed during

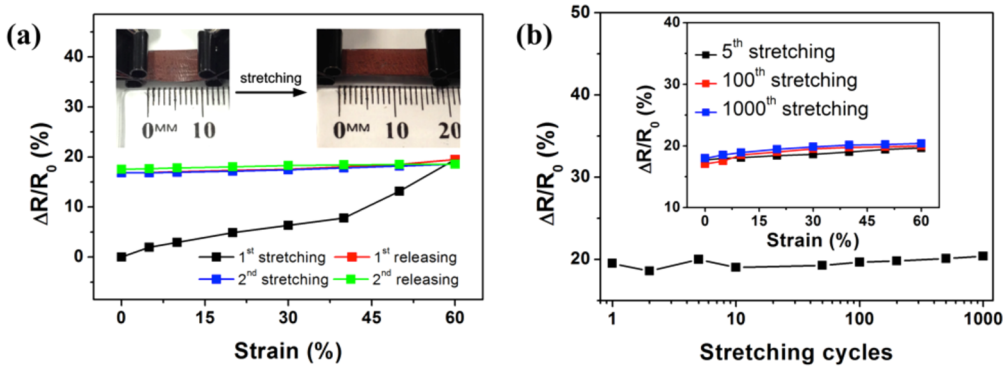

Figure 6. CuNW–PVA–PDMS rubber amber sheets as stretchable conductors. (a) Variation of the resistance of the rubber sheets as a function of tensile strain up to 60% in the first two stretch–release cycles. (b) Variation of the resistance of the rubber sheets as a function of stretching cycles at a strain of 60%. The inset showed the resistance changes for the 5th, 100th, and 1000th stretching cycles, respectively.

the PDMS embedding (Figure 5b and c). PDMS embedding substantially enhanced the compressive strength by 200-fold, up to a Young's modulus of 37.5 kPa (Figure S7). For the CuNW–PVA aerogel, repeated large strains could cause internal structural collapse, leading to a decrease of Young's moduli (Figure S8a,b). In contrast, the repeated compression under large strains for embedded aerogels did not show any observable changes in Young's moduli (Figure S8c,d). More importantly, the aerogel rubber ambers could be easily cut into arbitrary 1D, 2D, and 3D shapes (Figure 5d–f), and all the shaped rubbers were directly conductive without the need of prewiring. Similar conducting aerogel rubber was reported earlier, but prewiring was required.[1,13,27] The electrical conductivity of our rubber ambers was comparable to previous elastomeric conductors (Table S2). Moreover, the shaped rubber ambers could be further manufactured into various complex structures such as plaited and twisted structures. The outstanding mechanical compliance and electrical conductivity in conjunction with facile cut-shapeability enabled a prototype of the elastic piezoresistivity device (Figure S9 and supplementary video 2).

The conducting CuNWs rubber ambers also showed great potential as stretchable conductors. We sliced the rubber ambers into thin sheets and tested the variation of their normalized resistance ($\Delta R/R_0$) as a function of tensile strain from 0 to 60% (Figure 6a). In the first stretching cycle, the resistance increased 19.5% at a maximum strain of 60%; after releasing the load, a conductivity loss of 16.8% was observed. This could be attributed to partial breaking or cracking of the nanowire–PVA network.[33] Nevertheless, the resistance increase in our CuNWs rubber sheet was still lower than the reported values for carbon-based stretchable conductors.[34,35] For the second stretching cycle, only a ~0.7% change in conductivity was observed, and the change became negligible after the fifth stretching cycle (inset of Figure 6b). The conductivity reduced only ~1.2% after 1000 stretching cycles (Figure 6b).

CONCLUSIONS

In summary, we developed a cost-effective approach to fabricate a CuNW–aerogel-based stretchable conductor under mild conditions. The critical role of PVA was twofold: stabilizing CuNW scaffolds and substantially enhancing the mechanical robustness and flexibility of the aerogels. The CuNW–PVA aerogels could be further embedded into PDMS without noticeable deformation. PVA also played critical nanogluing roles in preventing the CuNWs from collapsing during embedding, enabling maintaining the high conductivity. Importantly, the resulting rubber ambers were conductive without the need for prewiring, and they could be manufactured into arbitrary complex 1D, 2D, and 3D shapes simply by cutting. All the shaped rubber ambers remained conductive. The outstanding electrical properties and mechanical compliance of both the CuNW–PVA aerogel and rubber ambers enabled prototypes of piezoresistive switches and stretchable conductors. We believe that our methodology represents a new low-cost approach to stretchable conductors and switches with a broad spectrum of applications such as in flexible touch displays, human–machine interfacing devices, and prosthetic skins.

MATERIALS AND METHODS

Materials. Copper(II) nitrate pentahemihydrate ($Cu(NO_3)_2 \cdot 2.5H_2O$, ≥98%), ethylenediamine (EDA, BioXtra), hydrazine solution (N_2H_4, 35 wt % in H_2O), polyvinylpyrrolidone (PVP, M_w = 10,000), and poly(vinyl alcohol) (PVA, M_w = 85 000–124 000) were purchased from Sigma-Aldrich. Sodium hydroxide (≥99.5%) was obtained from Merck. DuPont Solamet PV412 silver-based polymer conductive paste was purchased

from DuPont Microcircuit Materials. SYLGARD 184 silicon elastomer curing agent and SYLGARD 184 silicon elastomer base were obtained from Dow Corning. All of these chemicals were used as received.

Instruments. CuNW−PVA aqueous solutions were frozen by a Sanyo ultralow temperature freezer at −80 °C, and the freeze-drying process was performed on a HETO PowerDry PL6000 freeze-dryer. The dimensions of CuNW−PVA composite aerogels were measured by a Stamvick caliper with an accuracy of 0.01 mm, and the weights of the samples were checked with a Mettler Toledo balance (MS 105DU) with an accuracy of 0.01 mg. Scanning electron microscope (SEM) images of CuNW−PVA composite aerogels were taken on an FEI Nova NanoSEM 430 field emission gun scanning electron microscope operated at an acceleration voltage of 2 kV and a working distance of 4−5 mm. Mechanical properties of cylindrical-shaped CuNW−PVA composite aerogels were measured by a Micro Tester Instron (5848) using a 10 N load cell and strain control mode with a strain rate of 100% min^{-1}. The electrical conductivity of CuNW−PVA composite aerogels was measured through a two-probe technique. A thin layer of silver paste was employed to optimize the electrical contact between the CuNW−PVA composite aerogels and aluminum foils. The electrical resistance and the current variation with changing compressive strains were checked by a PARSTAT 2273 advanced electrochemical system (Princeton Applied Research).

Synthesis of CuNWs. NaOH (20 mL, 15 M), $Cu(NO_3)_2$ (1 mL, 0.1 M), EDA (0.15 mL), and N_2H_4 (0.025 mL, 35 wt %) were mixed in sequence and stirred at 200 rpm in a 50 mL round-bottom flask. Then, the solution was heated at 80 °C for 3 min. After the mixture turned colorless, it was poured into a 50 mL centrifuge tube immersed in an ice bath. Then, 5 mL of a PVP (0.4 wt %) aqueous solution was gently dropped on top of the reaction solution. After 1 h of aging in an ice bath, CuNWs floated on the top of the reaction solution. For purification, CuNWs were first redispersed in an aqueous washing solution (WS1) containing N_2H_4 (3 wt %) and PVP (1 wt %) and centrifuged at 2000 rpm for 5 min. Then, the precipitated CuNWs were redispersed in new WS1 by vortexing at 3000 rpm for 30 s. The purification process with WS1 was repeated three times to eliminate redundant reaction agents. To remove the excess PVP, CuNWs were redispersed in WS2 containing N_2H_4 (3 wt %) and centrifuged at 2000 rpm for 5 min twice. Finally, the superfluous hydrazine was eliminated by deionized water *via* centrifugation at 2000 rpm for 5 min.

Fabrication of CuNW−PVA Composite Aerogel. The mixture of CuNWs and PVA was pour into a sample vial (50 × 12 mm) and was left in a freezer at −80 °C for 2 h. Then, the frozen sample was freeze-dried at a sublimation temperature of −47.4 °C and a pressure of 0.10 KPa.

Fabrication of CuNW−PVA−PDMS Rubber Ambers. In the first step, PDMS was infiltrated into the CuNW−PVA composite aerogels. Briefly, precured PDMS, the mixture of the "base" and the "curing agent" with a ratio of 10:1, was gently poured onto the as-prepared CuNW−PVA composite aerogels. Then, the composite aerogels in precured PDMS were degassed in a desiccator for approximately 4 h, until no gas bubbles were observed on the surface of the mixture. PDMS encapsulation was completed by leaving the mixture in an oven at 80 °C for 2 h. In the second step, the CuNW−PVA−PDMS composites are cut into various 1D, 2D, and 3D morphologies with a blade.

Conflict of Interest: The authors declare no competing financial interest.

Supporting Information Available: Additional figures as described in the text (Figures S1−S9) are available. This material is available free of charge *via* the Internet at http://pubs.acs.org.

Acknowledgment. This work is financially supported ARC discovery projects DP120100170 and DP140100052. We also acknowledge Muhammad Muhaimin Yusman and Mohd Hariz Zainal Abidin. This work was performed in part at the Melbourne Centre for Nanofabrication (MCN) in the Victorian Node of the Australian National Fabrication Facility (ANFF).

REFERENCES AND NOTES

1. Ge, J.; Yao, H.-B.; Wang, X.; Ye, Y.-D.; Wang, J.-L.; Wu, Z.-Y.; Liu, J.-W.; Fan, F.-J.; Gao, H.-L.; Zhang, C.-L.; *et al*. Stretchable Conductors Based on Silver Nanowires: Improved Performance through a Binary Network Design. *Angew. Chem., Int. Ed.* **2013**, *125*, 1698–1703.
2. Xu, F.; Zhu, Y. Highly Conductive and Stretchable Silver Nanowire Conductors. *Adv. Mater.* **2012**, *24*, 5117–5122.
3. Liang, H.-W.; Guan, Q.-F.; Chen, L.-F.; Zhu, Z.; Zhang, W.-J.; Yu, S.-H. Macroscopic-Scale Template Synthesis of Robust Carbonaceous Nanofiber Hydrogels and Aerogels and Their Applications. *Angew. Chem., Int. Ed.* **2012**, *51*, 5101–5105.
4. Rogers, J.; Someya, T.; Huang, Y. Materials and Mechanics for Stretchable Electronics. *Science* **2010**, *327*, 1603–1607.
5. Sekitani, T.; Noguchi, Y.; Hata, K.; Fukushima, T.; Aida, T.; Someya, T. A Rubberlike Stretchable Active Matrix Using Elastic Conductors. *Science* **2008**, *321*, 1468–1472.
6. Rogers, J. A.; Bao, Z.; Baldwin, K.; Dodabalapur, A.; Crone, B.; Raju, V. R.; Kuck, V.; Katz, H.; Amundson, K.; Ewing, J.; *et al*. Paper-Like Electronic Displays: Large-Area Rubber-Stamped Plastic Sheets of Electronics and Microencapsulated Electrophoretic Inks. *Proc. Natl. Acad. Sci. U.S.A.* **2001**, *98*, 4835–4840.
7. Gelinck, G. H.; Huitema, H. E. A.; van Veenendaal, E.; Cantatore, E.; Schrijnemakers, L.; van der Putten, J. B. P. H.; Geuns, T. C. T.; Beenhakkers, M.; Giesbers, J. B.; Huisman, B.-H.; *et al*. Flexible Active-Matrix Displays and Shift Registers Based on Solution-Processed Organic Transistors. *Nat. Mater.* **2004**, *3*, 106–110.
8. Bae, S.; Kim, H.; Lee, Y.; Xu, X.; Park, J.-S.; Zheng, Y.; Balakrishnan, J.; Lei, T.; Ri Kim, H.; Song, Y. I.; *et al*. Roll-to-Roll Production of 30-Inch Graphene Films for Transparent Electrodes. *Nat. Nanotechnol.* **2010**, *5*, 574–578.
9. Someya, T.; Kato, Y.; Sekitani, T.; Iba, S.; Noguchi, Y.; Murase, Y.; Kawaguchi, H.; Sakurai, T. Conformable, Flexible, Large-Area Networks of Pressure and Thermal Sensors with Organic Transistor Active Matrixes. *Proc. Natl. Acad. Sci. U.S.A.* **2005**, *102*, 12321–12325.
10. Wang, C.; Hwang, D.; Yu, Z.; Takei, K.; Park, J.; Chen, T.; Ma, B.; Javey, A. User-Interactive Electronic Skin for Instantaneous Pressure Visualization. *Nat. Mater.* **2013**, *12*, 899–904.
11. Webb, R.; Bonifas, A.; Behnaz, A.; Zhang, Y.; Yu, K.; Cheng, H.; Shi, M.; Bian, Z.; Liu, Z.; Kim, Y.-S.; *et al*. Ultrathin Conformal Devices for Precise and Continuous Thermal Characterization of Human Skin. *Nat. Mater.* **2013**, *12*, 938–944.
12. Kim, D.-H.; Viventi, J.; Amsden, J. J.; Xiao, J.; Vigeland, L.; Kim, Y.-S.; Blanco, J. A.; Panilaitis, B.; Frechette, E. S.; Contreras, D.; *et al*. Dissolvable Films of Silk Fibroin for Ultrathin Conformal Bio-Integrated Electronics. *Nat. Mater.* **2010**, *9*, 511–517.
13. Chen, Z.; Ren, W.; Gao, L.; Liu, B.; Pei, S.; Cheng, H.-M. Three-Dimensional Flexible and Conductive Interconnected Graphene Networks Grown by Chemical Vapour Deposition. *Nat. Mater.* **2011**, *10*, 424–428.
14. Qiu, L.; Liu, J. Z.; Chang, S. L. Y.; Wu, Y.; Li, D. Biomimetic Superelastic Graphene-Based Cellular Monoliths. *Nat. Commun.* **2012**, *3*, 1241.
15. Garnier, F.; Yassar, A.; Hajlaoui, R.; Horowitz, G.; Deloffre, F.; Servet, B.; Ries, S.; Alnot, P. Molecular Engineering of Organic Semiconductors: Design of Self-Assembly Properties in Conjugated Thiophene Oligomers. *J. Am. Chem. Soc.* **1993**, *115*, 8716–8721.
16. Kim, D.-H.; Lu, N.; Ma, R.; Kim, Y.-S.; Kim, R.-H.; Wang, S.; Wu, J.; Won, S. M.; Tao, H.; Islam, A.; *et al*. Epidermal Electronics. *Science* **2011**, *333*, 838–843.
17. Fan, Z.; Ho, J. C.; Jacobson, Z. A.; Yerushalmi, R.; Alley, R. L.; Razavi, H.; Javey, A. Wafer-Scale Assembly of Highly Ordered Semiconductor Nanowire Arrays by Contact Printing. *Nano Lett.* **2007**, *8*, 20–25.
18. Sun, Y.; Rogers, J. A. Inorganic Semiconductors for Flexible Electronics. *Adv. Mater.* **2007**, *19*, 1897–1916.
19. Kim, Y.; Zhu, J.; Yeom, B.; Di Prima, M.; Su, X.; Kim, J.-G.; Yoo, S. J.; Uher, C.; Kotov, N. A. Stretchable Nanoparticle

Conductors with Self-Organized Conductive Pathways. *Nature* **2013**, *500*, 59–63.
20. Hu, L.; Kim, H. S.; Lee, J.-Y.; Peumans, P.; Cui, Y. Scalable Coating and Properties of Transparent, Flexible, Silver Nanowire Electrodes. *ACS Nano* **2010**, *4*, 2955–2963.
21. Chen, Y.; Ng, K. C.; Yan, W.; Tang, Y.; Cheng, W. Ultraflexible Plasmonic Nanocomposite Aerogel. *RSC Adv.* **2011**, *1*, 1265–1270.
22. Chen, Y.; Ouyang, Z.; Gu, M.; Cheng, W. Mechanically Strong, Optically Transparent, Giant Metal Superlattice Nanomembranes from Ultrathin Gold Nanowires. *Adv. Mater.* **2013**, *25*, 80–85.
23. Gong, S.; Schwalb, W.; Wang, Y.; Chen, Y.; Tang, Y.; Si, J.; Shirinzadeh, B.; Cheng, W. A Wearable and Highly Sensitive Pressure Sensor with Ultrathin Gold Nanowires. *Nat. Commun.* **2014**, *5*, 3132.
24. Yu, Y.; Zeng, J.; Chen, C.; Xie, Z.; Guo, R.; Liu, Z.; Zhou, X.; Yang, Y.; Zheng, Z. Three-Dimensional Compressible and Stretchable Conductive Composites. *Adv. Mater.* **2013**, *26*, 810–815.
25. Rathmell, A. R.; Wiley, B. J. The Synthesis and Coating of Long, Thin Copper Nanowires to Make Flexible, Transparent Conducting Films on Plastic Substrates. *Adv. Mater.* **2011**, *23*, 4798–4803.
26. Tang, Y.; Yeo, K. L.; Chen, Y.; Yap, L. W.; Xiong, W.; Cheng, W. Ultralow-Density Copper Nanowire Aerogel Monoliths with Tunable Mechanical and Electrical Properties. *J. Mater. Chem. A* **2013**, *1*, 6723.
27. Kim, K.; Vural, M.; Islam, M. Single-Walled Carbon Nanotube Aerogel-Based Elastic Conductors. *Adv. Mater.* **2011**, *23*, 2865–2869.
28. Yao, H.-B.; Huang, G.; Cui, C.-H.; Wang, X.-H.; Yu, S.-H. Macroscale Elastomeric Conductors Generated from Hydrothermally Synthesized Metal-Polymer Hybrid Nanocable Sponges. *Adv. Mater.* **2011**, *23*, 3643–3647.
29. Tappan, B. C.; Steiner, S. A.; Luther, E. P. Nanoporous Metal Foams. *Angew. Chem., Int. Ed.* **2010**, *49*, 4544–4565.
30. Estevez, L.; Kelarakis, A.; Gong, Q.; Da'as, E. H.; Giannelis, E. P. Multifunctional Graphene/Platinum/Nafion Hybrids *via* Ice Templating. *J. Am. Chem. Soc.* **2011**, *133*, 6122–6125.
31. Chelidze, T.; Gueguen, Y. Pressure-Induced Percolation Transitions in Composites. *J. Phys. D: Appl. Phys.* **1998**, *31*, 2877.
32. Yao, H.-B.; Ge, J.; Wang, C.-F.; Wang, X.; Hu, W.; Zheng, Z.-J.; Ni, Y.; Yu, S.-H. A Flexible and Highly Pressure-Sensitive Graphene—Polyurethane Sponge Based on Fractured Microstructure Design. *Adv. Mater.* **2013**, *25*, 6692–6698.
33. Liang, H.-W.; Guan, Q.-F.; Zhu, Z.; Song, L.-T.; Yao, H.-B.; Lei, X.; Yu, S.-H. Highly Conductive and Stretchable Conductors Fabricated from Bacterial Cellulose. *NPG Asia Mater.* **2012**, *4*, e19.
34. Kim, K. S.; Zhao, Y.; Jang, H.; Lee, S. Y.; Kim, J. M.; Kim, K. S.; Ahn, J.-H.; Kim, P.; Choi, J.-Y.; Hong, B. H. Large-Scale Pattern Growth of Graphene Films for Stretchable Transparent Electrodes. *Nature* **2009**, *457*, 706–710.
35. Chun, K.-Y.; Oh, Y.; Rho, J.; Ahn, J.-H.; Kim, Y.-J.; Choi, H. R.; Baik, S. Highly Conductive, Printable and Stretchable Composite Films of Carbon Nanotubes and Silver. *Nat. Nanotechnol.* **2010**, *5*, 853–857.